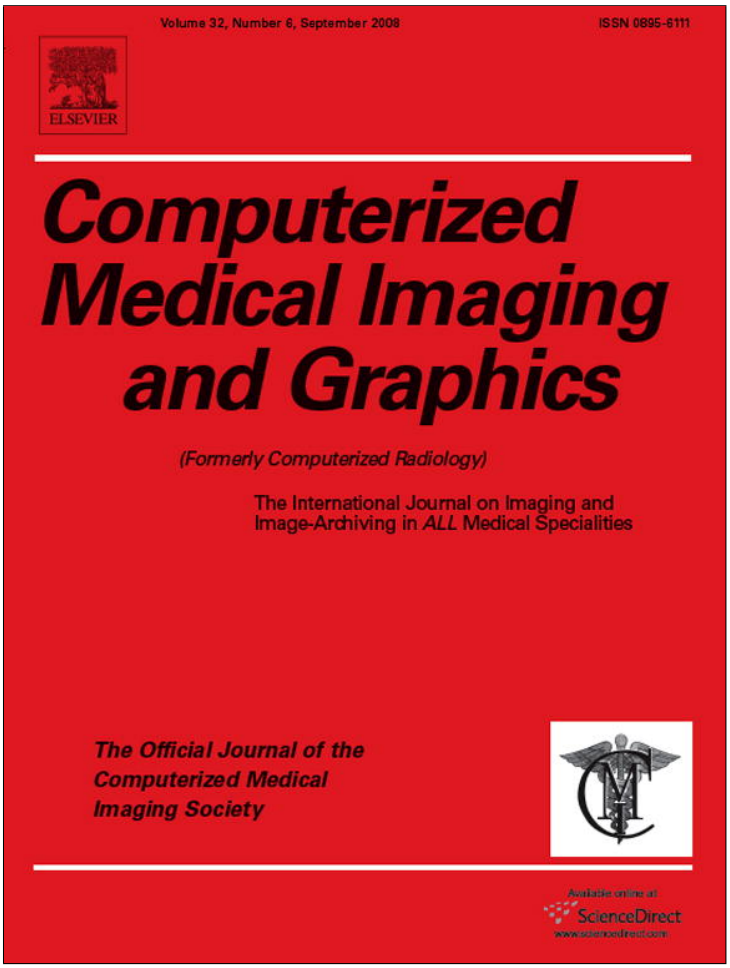

Available online at www.sciencedirect.com
ScienceDirect
Computerized Medical Imaging and Graphics 32 (2008) 513–520
Computerized Medical Imaging and Graphics
www.elsevier.com/locate/compmedimag

Medical image analysis of 3D CT images based on extension of Haralick texture features

Ludvík Tesař[a,*], Akinobu Shimizu[b,1], Daniel Smutek[c,2], Hidefumi Kobatake[d,3], Shigeru Nawano[e,4]

[a] *Institute of Information Theory and Automation, Czech Academy of Sciences, Department of Adaptive Systems, Pod Vodarenskou Vezi 4, 18208 Praha 8, Czech Republic*
[b] *Tokyo University of Agriculture and Technology, Shimizu Laboratory, 2-24-16 Naka-cho, Koganei-shi, Tokyo 184-8588, Japan*
[c] *3rd Dept of Medicine, Charles University 1st Medical Faculty, U nemocnice 1, 128 08 Praha 2, Czech Republic*
[d] *Tokyo University of Agriculture and Technology, 3-8-1 Harumi-cho, Fuchu-shi, Tokyo 183-8538, Japan*
[e] *International University of Health and Welfare, 1-4-3 Mita Minato-ku, Tokyo 108-8329, Japan*

Received 26 September 2007; received in revised form 12 May 2008; accepted 27 May 2008

Abstract

Purpose: A new approach to the segmentation of 3D CT images is proposed in an attempt to provide texture-based segmentation of organs or disease diagnosis. 3D extension of Haralick texture features was studied calculating co-occurrences of all voxels in a small cubic region around the voxel.
Results: For verification, the proposed method was tested on a set of abdominal 3D volumes of patients. Statistically, the improvement in segmentation was significant for most of the organs considered herein.
Conclusions: The proposed method has potential application in medical image segmentation, including diagnosis of diseases.

Keywords: Haralick texture features; 3D image analysis; Image segmentation; Gaussian mixture model; Model-based decision-making; EM algorithm

1. Introduction

Texture-based image analysis using medical images has been investigated both theoretically and practically. In the present study, we investigate 3D images using texture features. Interest in this subject has grown as CT and MRI scans have become cheaper, making more images available for treatment. Specifically, we study new possibilities for texture feature-based analysis that have come about with the availability of 3D images.

Texture features are often used for image analysis [1], especially for medical images. Texture features are calculated from given image region pixels in order to characterize the texture of that region. Haralick texture features are commonly used in 2D texture analysis of medical images [2–4]. In the present study, we examined a specific 3D extension of Haralick features for effective segmentation of three-dimensional CT scans of the abdominal area. In order to verify the usability of the proposed extension of 3D Haralick texture features, segmentation of abdominal area was performed. Segmentation was performed with model-based learning and maximum likelihood decision-making [2,5,6]. The model applied herein is a Gaussian mixture model. The standard EM algorithm was used for estimation of the model's parameters [7].

In Section 2 we describe the specific implementation of Haralick texture features in the 3D domain for 3D CT, MRI, or any other 3D images available. The contribution of the present paper is to determine whether this implementation of Haralick texture features provides a statistically significant improvement in segmentation. In Section 3, we describe a method for segmentation

* Corresponding author. Tel.: +420 266052583; fax: +420 266052068.
E-mail addresses: tesar@utia.cas.cz (L. Tesař), simiz@cc.tuat.ac.jp (A. Shimizu), smutek@cesnet.cz (D. Smutek), kobatake@cc.tuat.ac.jp (H. Kobatake), snawano@iuhw.ac.jp (S. Nawano).
[1] Tel.: +81 42 388 7478; fax: +81 42 388 7478.
[2] Tel.: +420 224962958; fax: +420 224919780.
[3] Tel.: +81 42 367 5000.
[4] Tel.: +81 3 3451 8121; fax: +81 3 3454 0067.

0895-6111/$ – see front matter © 2008 Elsevier Ltd. All rights reserved.
doi:10.1016/j.compmedimag.2008.05.005

based on proposed features. Section 4 shows an example of medical data segmentation. CT data of abdominal part of the human body were segmented using 3D features.

The entire image contains additional information that is not possible to obtain from the texture. Also, statistical assessment is performed as to whether the new 3D features actually provide new information that can be used for the segmentation of actual images.

2. Extension of Haralick features to the 3D domain

Haralick 2D texture features are statistics calculated from a co-occurrence matrix. This matrix is computed from pixel intensity values (from an image-analysis point of view these are gray-level values of images, and in the case of CT, the gray-level represents the CT value) in a given region. The co-occurrence matrix is frequently used in image analysis because it represents important characteristics of the texture in a given region. Haralick features are statistics defined to emphasize certain texture properties. The co-occurrence matrix consists of numbers that are the co-occurrence counts of the same gray-scale color (intensity) in two pixels separated by an oriented separation vector. The number of intensity values must be finite and relatively small in order to contain any co-occurrences in the co-occurrence matrix. The number of intensity values is called the "quantization constant" and is denoted by q.

2.1. Definition of co-occurrence matrix in the 2D and 3D domains

We define the original 2D or 3D image by (two- or three-dimensional) intensity array P with intensities $p_{\vec{v}}$ quantized to q intensity classes (i.e. $p_{\vec{v}}$ have one of q values). Vector $\vec{v}$ is two- or three-dimensional vector $\vec{v}$ which is called pixel (in 2D case) and voxel (in 3D case). Co-occurrence matrix $C_{\vec{v}}^{(\vec{s})}$ is defined by its components $c_{\vec{v}}^{(\vec{s})}(i, j)$. The separation vector is two- or three-dimensional vector $\vec{s}$. Window $W(\vec{v})$ of size $2w + 1$ around $\vec{v}$ is defined as follows:

$$W(\vec{v}) = \{\vec{u} \in I : \vec{v} - \vec{w} \leq \vec{u} \leq \vec{v} + \vec{w}\} \quad (1)$$

where $\vec{w} = (w, w)$ for 2D and $\vec{w} = (w, w, w)$ for 3D image. I is the set of pixels (or voxels) that represents the entire image region of interest. The co-occurrence matrix is defined as follows:

$$c_{W(\vec{v})}^{(\vec{s})}(i, j) = \frac{|\{\vec{u} \in W(\vec{v}) : \vec{u} + \vec{s} \in I; p_{\vec{u}} = i; p_{\vec{u}+\vec{s}} = j\}|}{|W(\vec{v})|} \quad (2)$$

The lack of symmetry in definition of $C_{\vec{v}}^{(\vec{s})}$ is dealt with by averaging over all major directions, as mentioned at the end of Section 2. This approach is also used in Section 4.

Note that the original Haralick texture features defined in [3,8] are defined region-wise, as if $W(\vec{v})$ in Eq. (2) was the region of interest of the image (i.e. part of the image that is suspected to have the same texture pattern). Here we are considering the matrix $C_{\vec{v}}^{(\vec{s})}$ to represent the texture around individual pixel (or voxel) $\vec{v}$.

2.2. Definition of Haralick texture features

After co-occurrence matrix C with components $c(i, j)$ is calculated, Haralick features can be computed using the formulas below. First, however, the statistics must be defined:

$$\mu_x = \sum_{i=1}^{q}\sum_{j=1}^{q}(i-1)c(i, j)$$

$$\mu_y = \sum_{i=1}^{q}\sum_{j=1}^{q}(j-1)c(i, j)$$

$$var_x = \sum_{i=1}^{q}\sum_{j=1}^{q}(i-1-\mu_y)^2 c(i, j)$$

$$var_y = \sum_{i=1}^{q}\sum_{j=1}^{q}(j-1-\mu_y)^2 c(i, j)$$

$$c_{x-y}(k) = \sum_{j=1}^{q}\sum_{i \in \{1,\ldots,q\};|i-j|=k-1} c(i, j)$$

where $c_{x+y}(k)$ is defined for $k = 1, 2, \ldots, 2q-1$ and $c_{x-y}(k)$ for $k = 1, \ldots, q$.

The Haralick features considered in the preset paper is as follows:

Entropy:

$$-\sum_{i=1}^{q}\sum_{j=1}^{q}c(i, j)\log c(i, j)$$

Texture contrast:

$$\sum_{i=1}^{q}\sum_{j=1}^{q}|i-j|c(i, j)$$

Texture correlation:

$$\sum_{i=1}^{q}\sum_{j=1}^{q}\frac{(i-1-\mu_x)(j-1-\mu_y)c(i, j)}{\sqrt{\mathrm{var}_x \mathrm{var}_y}}$$

Texture homogeneity:

$$\sum_{i=1}^{q}\sum_{j=1}^{q}\frac{c(i, j)}{1+|i-j|}$$

Inverse difference moment:

$$\sum_{i=1}^{q}\sum_{j=1,\ldots,q;j\neq i}\frac{c(i, j)}{|i-j|}$$

Maximum probability:

$$\max_{i=1,\ldots,q;j=1,\ldots,q} c(i, j)$$

Contrast:

$$\sum_{i=1}^{q}(i-1)^2 c_{x-y}(i)$$

Difference entropy:

$$-\sum_{i=1}^{q} c_{x-y}(i)\log(c_{x-y}(i))$$

The total number of Haralick texture features considered here is 8. Additional features are described in previous studies [3,8]. For present data, additional Haralick texture features have strong correlation with the features defined above. Features removed due to the strong correlation are namely: uniformity of energy, sum average, sum entropy, variance, information measure of correlation, maximal correlation coefficient. For several of features, division by zero may occur. Such cases must be dealt with. For a few features, defining 0 log 0 to be equal to its limit, 0, may help. In other cases, adding a very small value to the denominator is an acceptable technical solution.

The Haralick texture features presented herein can be further parameterized by three parameters: separation vector $\vec{s}$, quantization constant q, and window size w. We focus herein on isotropic texture so that only the absolute value of the separation vector $\vec{s}$, and not its direction, is important. Co-occurrence matrices can be calculated for all six major directions in 3D space (up, down, left, right, forward, and backward), and then averaged (as suggested by Haralick [8]). This approach adds more data, which makes such co-occurrence matrix a better statistic for the underlying texture.

2.3. Advantages of 3D texture features

Haralick features are statistics that are computed from the co-occurrence matrix C. As originally presented by Haralick [8], and used widely thereafter, the co-occurrence matrix is generated from all of the data in the region of interest R (or in the entire image), in order to evaluate the overall properties of the texture in the entire region. Since we are investigating the possibility of obtaining co-occurrence matrix-based Haralick features locally for each pixel, we calculate this matrix on a reasonable small window around each pixel of the image. Therefore, the co-occurrence matrix and the features can be calculated for each pixel of the image. The problem with this approach is that the co-occurrence matrix must be filled with reasonably large values from a statistical point of view. Otherwise, the matrix does not distinguish different regions well. Therefore, the window size around the pixel of interest should be relatively large. However, if the window size is too large, then even distant pixels influence features belonging to the pixel of interest, which means that, for bigger windows, features will be blurred. To illustrate the concept of the size of the window, Figs. 1 through 4 compare the window-based Haralick features for different window sizes.

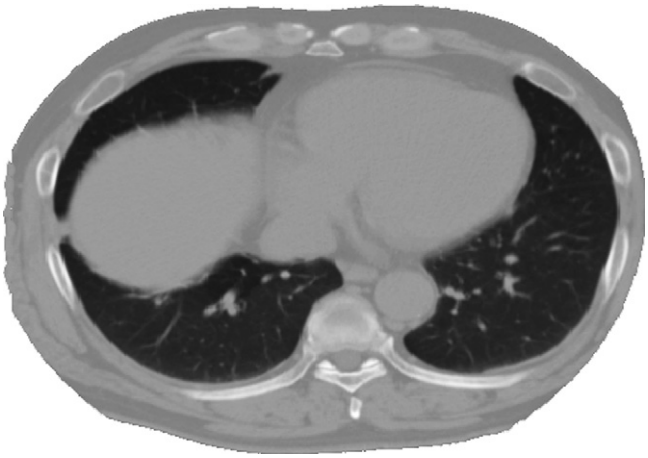

Fig. 1. CT scan layer of an abdominal part of the human body (size: 512 × 512).

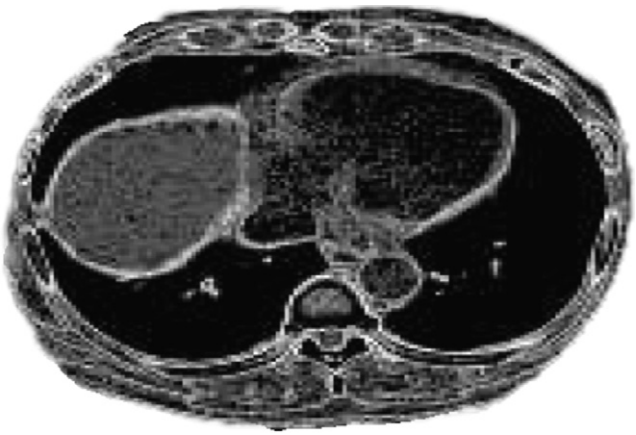

Fig. 2. Haralick feature (entropy) calculated for the image in Fig. 1. Window size, $w = 1$, quantization constant $q = 8$ (size: 512 × 512).

In the 2D case, the window size will either have insufficient size to produce useful Haralick features or will be too large and so will produce a blurred feature image. However, the concept of local co-occurrence features and local images can be applied much more effectively to 3D images. In the 3D case, the window area can be made large enough to fill a co-

Fig. 3. Haralick feature (entropy) calculated for the image in Fig. 1. Window size $w = 2$, quantization constant $q = 8$ (size: 512 × 512).

Fig. 4. Haralick feature (entropy) calculated for the image in Fig. 1. Window size $w = 4$, quantization constant $q = 8$ (size: 512 × 512).

occurrence matrix of reasonable size. We employ the fact that, in 3D space, there are many more voxels around the diameter d of a given voxel (proportional to d^3) than in the 2D space (where the number of pixels is proportional to d^2). Hence, the amount of information about texture, which is proportional to the number of voxels or pixels in such surroundings, is also higher in 3D space. Thus, while co-occurrence-based features such as Haralick features in the 2D domain are only useful for describing texture in larger areas of the image, in 3D images, these features can be used to characterize smaller areas around every single voxel.

3. Use of 3D Haralick texture features for image segmentation

Texture features are statistics that can distinguish between different types of image texture. In this section, we describe the actual method used for image segmentation, which employs the features discussed in Section 2. The method described here uses a database of 3D images that have known segmentation. Specifically, the type of tissue of each voxel of the 3D image is known. The segmentation algorithm learns the value of features for every type of tissue under consideration. This is called the "learning phase" and is described in Section 1. Features are fitted to the given parameterized model, and for every tissue type a different set of parameters is provided. This is the why this approach is also referred to as model-based. Segmentation of an unknown image is performed in the "inference phase", as described in Section 2. For every voxel, decision-making is performed using the parameterized models in the learning phase. The inference is based on the maximum likelihood.

3.1. Learning phase

We assume m types of tissue indexed by $t = 1, 2, \ldots, m$. Let the voxel at coordinates $\vec{v}$ belong to tissue type t. This will be denoted as $M(\vec{v}) = t$. Feature vector $f(\vec{v})$ is assumed to be a random variable with a given conditional probability density function (pdf) conditioned by the value of $M(\vec{v})$. The model for feature $f(\vec{v})$ is then defined as:

$$p(f(\vec{v})|M(\vec{v}) = t) = \sum_{k=1}^{n} \frac{\alpha_k(t)}{(2\pi)^{d/2}|C_k(t)|^{1/2}} \times \exp\left[-\frac{1}{2}(f(\vec{v}) - \mu_k(t))^T C_k^{-1}(t)(f(\vec{v}) - \mu_k(t))\right] \quad (3)$$

where $p(f(\vec{v}))$ is the multi-dimensional pdf of feature vector $f(\vec{v})$ of the voxel in the region with tissue type t, n is the number of components of the mixture, $\alpha_k(t)$, $C_k(t)$, and $\mu_k(t)$, are unknown parameters of the Gaussian mixture that are estimated by the EM algorithm in the learning step, and d is the dimension of the feature vector.

Pdf $p(f(\vec{v}))$ is the model for feature vector $f(\vec{v})$. The goal of the learning phase is to find the estimate for the set of parameters $\alpha_k(t)$, $C_k(t)$, and $\mu_k(t)$ for given data $f(\vec{v})$ from the abovementioned database of known labels.

The optimal value for parameter n (which is the number of Gaussian pdf's in the mixture) must be found. As the speed of calculation decreases with the size of n, the accuracy of segmentation generally grows slightly with n, compromise is necessary in order to achieve reasonable accuracy of segmentation in reasonable time. This is realized in the application described in Section 4.

3.2. Inference phase

Inference is performed for every voxel in the image to be segmented. The pdf value $p(f(\vec{v})|M(\vec{v}) = t)$ is calculated for every image and for every type of tissue t. As a result, for every feature vector $f(\vec{v})$, pdf values $p(f(\vec{v})|M(\vec{v}) = 1)$, $p(f(\vec{v})|M(\vec{v}) = 2), \ldots, p(f(\vec{v})|M(\vec{v}) = m)$ represent likelihoods, and the estimated tissue type is found by maximization over all m tissue type labels.

3.3. A note on merging results with different probabilistic methods

It is assumed that the method described herein would be combined with another segmentation method to achieve successful segmentation. As demonstrated herein, the information included in texture allows an image to be segmented. However, medical images can contain several other sources of information, some of which have probabilistic form. This means that the results of the other methods have the form $p(M(\vec{v}) = t)$. These results can be used as prior information for the present method, and posterior information will be given by Bayes' theorem:

$$p(M(\vec{v}) = t|f(\vec{v})) \propto p(f(\vec{v})|M(\vec{v}) = t)p(M(\vec{v}) = t) \quad (4)$$

Symbol $\propto$ denotes proportionality. Instead of maximizing the likelihood, the result is obtained by maximizing the posterior probability function over all models.

As an example of good prior information, a probabilistic atlas of organs can be taken [9].

4. Results in medical CT data segmentation

The problem of organ segmentation of the abdominal part of the body based on non-contrast CT was considered. Segmentations with and without Haralick texture features were compared. A test was performed in order to determine whether such specialized texture features improve segmentation and whether this improvement is statistically significant. The hypothesis is that each pattern has its own specific texture pattern, which is advantageous for segmentation, as compared to segmentation based only on basic texture features, such as the raw CT value or its gradient.

The available data are described as follows. Organ segmentation was known in advance for all 10 subjects. CT images were obtained using a multi-detector CT with a voltage of 120 kV. The image size was $512 \times 512 \times 400$, where 400 is only approximate value since it varies with each subject. The images were isotropic, and the voxel size was 0.5 mm in all three dimensions. Segmentation of organs by hand was performed for each subject (label images) and approved by medical doctor. The original size of the label images is the same as the size of CT images. Six organs were considered for segmentation, which makes a total of seven models (one model for the case of a non-target organ). The selected organs were the liver, the spleen, the kidneys, the heart + aorta + inferior vena cava (i.v.c.), the digestive fluid in the stomach, and the stomach wall. For the purpose of Haralick features calculation, data were quantized for CT values of -110 to 190 (Hounsfield units) because most abdominal cavity organs have intensities in this interval. This is not true for the bones and lungs, which makes these two organs especially easy to segment by other trivial methods, like thresholding, so they were extracted in advance. Organs that contain mostly blood, such as the heart, the aorta, and the inferior vena cava, should have the same pattern. Since the ability to distinguish patterns was tested, such organs were assembled into the same model. On the other hand, the stomach was divided into the digestive fluid in stomach and the stomach wall, because these two regions of the same organ have clearly different texture patterns. In order to reduce computational cost, segmentation was performed on the grid $170 \times 170 \times 130$, which is approximately one third of the original grid. Original label images were down-sampled to the same size for comparison.

For comparison, segmentation was performed using the same method, but with only six basic texture features;

- original CT value;
- absolute value of the gradient of CT values;
- absolute value of the second moment of the CT value computed as the norm of the vector made from the second moment in every dimension (each second moment is a function of three adjacent voxels);
- normalized 3D coordinates x, y, and z in the abdominal cavity were taken as three additional features;

In addition, a probabilistic atlas of organs [9] was used as prior information in the inference phase of segmentation, as described in Section 3.

In order to evaluate the contribution of Haralick features, the segmentation was performed with six basic features from the comparison set and Haralick features were added to the feature vector. Only a subset of Haralick features was selected. This subset was selected by removing the features with strong correlation with other features for given data. A set of eight Haralick texture features was used, the names of which are given in Section 2 as entropy, texture contrast, texture correlation, texture homogeneity, inverse difference moment, maximum probability, contrast, and difference entropy. Co-occurrences were calculated with all separation vectors having the Euclidean norm equal to 1 (separation vectors have integer elements only, so there are six separation vectors in three-dimensional space). The window size was $w = 2$, which indicates that the co-occurrences were calculated on a cube of size $5 \times 5 \times 5$. The number of members in the Gaussian mixture was selected in order to maximize the segmentation performance. Multiple possibilities, between one and 13 members, were tested. A higher number of mixtures was not considered because the computation penalty was too high. Finally, nine members were selected as the most efficient choice.

The fivefold cross-validation method was used for evaluation. For each iteration, learning was performed with eight subjects. Thus, their known segmentation was employed, and two subjects were used for verification. Their known segmentation was compared with automatic segmentation. By repeating this five times, evaluation of all 10 subjects was performed.

To assess the effectiveness of segmentation, we used the degree of correspondence, which is the proportion of size of the intersection and the union of the known correct segmentation and the automatic segmentation achieved by the algorithm. This was performed for all test subjects and each organ. A single-tailed paired-sample t-test, was used to compare two sets of results for each organ. The null hypothesis was that there was no improvement in segmentation. The significance level was 0.05.

Fig. 5 shows one layer from the original 3D image. Fig. 6 shows the gold-standard segmentation of organs in Fig. 5, as approved by a medical doctor. One gray scale value is used to indicate every organ. Using the basic features, this image was

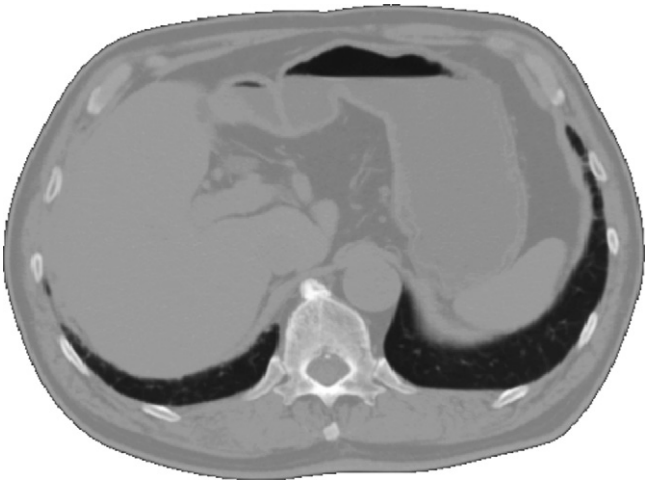

Fig. 5. One layer from the original 3D image (size: 512×512).

Fig. 6. Hand-made organ labels for the layer in Fig. 5 (size: 170 × 170).

Fig. 7. Automatically generated organ labels for the layer in Fig. 5 using basic features (size: 170 × 170).

segmented as in Fig. 7. With Haralick features, the obtained segmentation is shown in Fig. 8. This is a typical segmentation of the image. When only basic features were used, there were more mis-detections. For example, part of the stomach was mis-identified as the liver, or the extracted aorta was too large as compared to true aorta. We performed a statistical test to determine whether this difference is statistically significant.

The graph in Fig. 9 shows the comparison of the degree of correspondence between organs. In the statistical test performed organ-wise, significant improvement was obtained for all organs, except for the kidney, for which some improvement was observed, although it was not statistically significant. Table 1 sums the results. Summing the results for all organs, the improvement was also significant, with a p-value of 3.2×10^{-5}.

Fig. 8. Automatically generated organ labels for the layer in Fig. 5 using Haralick co-occurrence matrix-based texture features (size: 170 × 170).

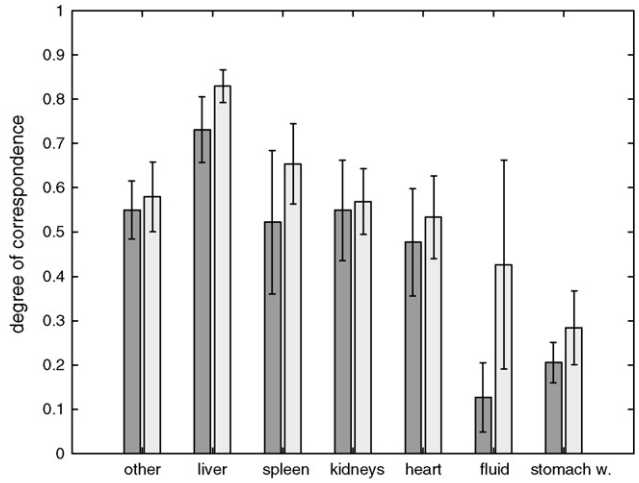

Fig. 9. Graph with per-organ comparison of degree of correspondence of classification for the cases with (light gray) and without Haralick features (dark). The organs include 'other organs', the liver, spleen, kidneys, heart with aorta and i.v.c., digestive fluid in stomach, and stomach wall. Vertical strokes indicate standard deviation.

Improvement in segmentation was observed for all organs. When assessing the improvement statistically, we found that the improvement was statistically significant for all organs except for the kidney. The reason why texture features contributed less to the segmentation of this organ might be a specific spatial distribution of different tissue patterns in this organ. The structure of the kidney has a somewhat fractal nature, with a greater number of levels of complexity (with different Hausdorff dimensions in different parts of the organ [10]), resulting in several different textures. In this organ, the pattern changes continuously with the level of complexity of the organ. Consequently, the diversity of texture features may be too high throughout the organ.

The present paper evaluates the sensitivity of the proposed features for different types of tissues with potential application in medical image diagnosis. Unexpectedly, a tumor was found inside of the liver tissue of one of the subjects (Figs. 10–13) and was classified as "other tissue" (see Fig. 13), distinguishing the tumor from the liver tissue. The tumor was found using Haralick texture features (Fig. 13) rather than the basic features (Fig. 12), indicating the document sensitivity of the co-occurrence texture features and the relative difficulty in locating this tumor on the

Table 1
t-Test results

Organ	t-Test result	p-Value ($\times 10^{-4}$)
Other organs	1	2.58
Liver	1	28
Spleen	1	2.85
Kidneys	0	1280
Heart + aorta + i.v.c.	1	190
Digestive fluid	1	6.11
Stomach wall	1	25

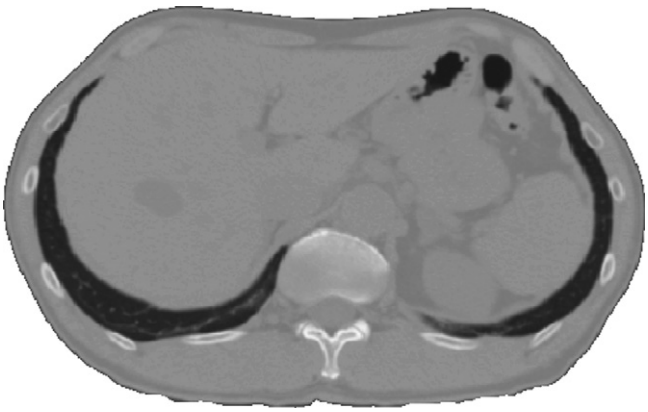

Fig. 10. One layer from the original 3D image (size: 512 × 512).

Fig. 11. Hand-made organ labels for the layer in Fig. 10 (size: 170 × 170).

Fig. 12. Automatically generated organ labels for the layer in Fig. 10 using basic features (size: 170 × 170).

original non-contrast CT image. In a statistical significance test, this was counted as an incorrect result, although the method has potential application in automatic disease diagnosis.

5. Discussion

In the present paper, a method for medical image segmentation in 3D space based on Haralick texture features was proposed. The proposed method is explained theoretically and gives good segmentation results. For verification, the proposed method was tested on a set of abdominal 3D volumes of patients.

Fig. 13. Automatically generated organ labels for the layer in Fig. 10 using Haralick co-occurrence matrix-based texture features. This figure indicates the ability to find a tumor based on differences in the texture of the tissue (size: 170 × 170).

Statistically, the improvement in segmentation was significant for most of the organs considered herein.

The proposed method has potential application in medical image segmentation, including diagnosis of diseases that change the texture of the part of the organ.

Acknowledgements

This work was supported by a Grant-in-Aid for Scientific Research on Priority Areas from the Ministry of Education, Culture, Sports, Science and Technology of Japan and by project 1ET101050403 of the Czech Academy of Sciences and by project 1M0572 of MSMT, Czech Republic.

References

[1] Muzzolini R, Yang YH, Pierson R. Texture characterization using robust statistics. Pattern Recognit 1994;27(1):119–34.
[2] Tesař L, Smutek D. Bayesian classification of sonograms of thyroid gland based on Gaussian mixtures. In: Proceedings of Norvegian conference on image processing and pattern recognition, NOBIM 2004. 2004. p. 36–40.
[3] Haralick RM, Shapiro LG. Computer and robot vision, vol. 1. Reading MA: Addison-Wesley Publishing Company; 1993. pp. 453–508.
[4] Smutek D, Šára R, Jiskra J, Tesař L. Ultrasound of thyroid gland—what is hidden inside and physician does not see. In: Cikes, Nada, editors. Lijecnicki Vjesnik; abstracts from European congress on ultrasound in medicine and biology 126 (Suppl. 2). Zagreb: Kratis; 2004. p. p. 57.
[5] Tesař L, Smutek D, Jiskra J, Maruna P. Learning and diagnostics of lymphocytic thyroiditis based on sonogram images. In: Shokin Yu I, Potaturkin OI, editors. Proceedings of the second IASTED international multi-conference on automation, control, and information technology. Calgary, Canada: ACTA Press; 2005. p. 316–9.
[6] Tesař L, Smutek D. Ultrasonography diagnostics using Gaussian mixture model. In: Proceedings of the 6TH international PhD workshop on systems and control, young generation viewpoint. 2005.
[7] Dempster AP, Laird NM, Rubin DB. Maximum likelihood from incomplete data via the EM algorithm. J R Stat Soc 1977;39:1–38.
[8] Haralick RM. Statistical and structural approaches to texture. Proc IEEE 1979;67(5):786–804.
[9] Shimizu A, Ohno R, Ikegami T, Kobatake H, Nawano S, Smutek D. Multi-organ segmentation in three dimensional abdominal CT images. In:

Proceedings of international journal of computer assisted radiology and surgery, CARS 2006. 2006. p. 76–8.
[10] Mandelbrot BB. The fractal geometry of nature. W.H. Freeman and Company; 1982.

Dr. Ludvik Tesar was born in Mlada Boleslav, Czechoslovakia in 1970. He received a degree from the Czech Technical University, in 1994 and a PhD, from the same University, in 1999. He was working at Trinity College, Dublin, Ireland and in Tokyo University of Agriculture and Technology, Tokyo, Japan. Since 2007, he has been with the Academy of Sciences of the Czech Republic, where he is a researcher. His research interests focus on medical image analysis and image segmentation.

Prof. Akinobu Shimizu received the BE, ME and PhD degrees from Graduate School of Engineering, Nagoya University in 1989, 1991 and 1995, respectively. From 1994 to 1998, he was a research associate at Nagoya University. Since 1998, he has been with the Tokyo University of Agriculture and Technology, where he is now an associate professor at the Graduate School of Engineering. His research activities are in the areas of image processing, pattern recognition and the applications to computer-aided diagnosis. He has received several awards, including 1994, 1996 and 2005 Best Paper Awards of Medical Imaging Technology. He is the member of the IEEE, the Institute of Electronics, Information and Communication Engineers, the Information Processing Society of Japan, the Japanese Society for Medical and Biological Engineering, the Japanese Society of Medical Imaging Technology, and the Japanese Society of Computer Aided Diagnosis of Medical Images.

Dr. Daniel Smutek was born in 1974 in Prague, Czechoslovakia. He received MD and PhD degree at Medical Faculty, Charles University, Prague, Czech Republic. Then he was working at Trinity College, Dublin, Ireland and in VTT, Tampere, Finland. Currently he works as an assistant professor at Charles University, Prague. His main fields of interests are medical image analysis and ultrasound imaging.

Prof. Hidefumi Kobatake received the BE, ME, and PhD degrees from University of Tokyo, Tokyo, Japan, in 1967, 1969 and 1972, respectively. From 1972 to 1975, he was a research associate at the Institute of Space and Aeronautical Science, University of Tokyo. Since 1975, he has joined Tokyo University of Agriculture and Technology, Tokyo, Japan, where he is now a president. His research activities include areas of acoustic signal processing, image processing, and pattern recognition. He is the author of books on speech precognition, digital signal processing, mathematical morphology and so on. He has received several awards, including 1987 Best Monograph Award from Society of Instrument and Control Engineering (SICE) and Best Paper Award of 1998 Three-Dimensional Image Conference. He is the member of IEEE, SICE, the Institute of Electronics, Information and Communication Engineers, the Japanese Society for Medical and Biological Engineering, the Society of Medical Imaging Technology, and the Society of Computer Aided Diagnosis of Medical Images, etc.

Dr. Shigeru Nawano graduated from the School of Medicine, Chiba University, in 1981. He became a research associate at Chiba University Hospital in 1982. He moved to the Diagnostic Radiology Division, National Cancer Center Hospital, in 1986. He was Chief of the Radiology Division, National Cancer Center Hospital East, since 1992. He moved to International University of Health and Welfare in 2007. His research interests include computed radiography, mammography, CAD, MRI, and CT. He holds MD/PhD degrees.